



HAL
open science

Paleogeographic differences in temperature, water depth and conodont biofacies during the Late Devonian

Catherine Girard, Jean-Jacques Cornée, Michael Joachimski, Anne-Lise Charruault, Anne-Béatrice Dufour, Sabrina Renaud

► To cite this version:

Catherine Girard, Jean-Jacques Cornée, Michael Joachimski, Anne-Lise Charruault, Anne-Béatrice Dufour, et al.. Paleogeographic differences in temperature, water depth and conodont biofacies during the Late Devonian. *Palaeogeography, Palaeoclimatology, Palaeoecology*, 2020, 549, pp.108852. 10.1016/j.palaeo.2018.06.046 . hal-04614741

HAL Id: hal-04614741

<https://hal.science/hal-04614741>

Submitted on 17 Jun 2024

HAL is a multi-disciplinary open access archive for the deposit and dissemination of scientific research documents, whether they are published or not. The documents may come from teaching and research institutions in France or abroad, or from public or private research centers.

L'archive ouverte pluridisciplinaire **HAL**, est destinée au dépôt et à la diffusion de documents scientifiques de niveau recherche, publiés ou non, émanant des établissements d'enseignement et de recherche français ou étrangers, des laboratoires publics ou privés.

1 **Paleogeographic differences in temperature, water depth and conodont biofacies**
2 **during the Late Devonian**

3
4 Girard, Catherine^{1,*}, Cornée, Jean-Jacques^{2,3}, Joachimski, Michael M.⁴, Charruault, Anne-
5 Lise¹, Dufour, Anne-Béatrice⁵, Renaud, Sabrina⁵

6
7 ¹ Institut des Sciences de l'Evolution, Université de Montpellier, UMR5554 CNRS, IRD,
8 EPHE, Place Eugène Bataillon, CC65, 34095 Montpellier cedex, France
9 (catherine.girard@umontpellier.fr; anne-lise.charruault@umontpellier.fr)

10 ² Géosciences Montpellier, Université de Montpellier, 34095 Montpellier Cedex 05,
11 France (jean-jacques.cornee@gm.univ-montp2.fr)

12 ³ current address : Université des Antilles, Campus de Fouillole, 97170 Pointe-à-Pitre,
13 France

14 ⁴ GeoZentrum Nordbayern, University of Erlangen-Nuremberg, Schlossgarten 5, D-
15 91054 Erlangen, Germany (michael.joachimski@fau.de)

16 ⁵ Laboratoire de Biométrie et Biologie Evolutive, UMR 5558, Université de Lyon,
17 Université Lyon 1, CNRS, 69100 Villeurbanne, France (sabrina.renaud@univ-lyon1.fr;
18 anne-beatrice.dufour@univ-lyon1.fr)

19
20 *corresponding author

21
22 **Abstract**

23
24 The Famennian (Late Devonian) started after and ended with two of the seven largest
25 crises of the Phanerozoic, the Kellwasser and Hangenberg events, respectively. In
26 between, global environmental trends have been identified, involving cooling and
27 eustatic regression. Tropical and subtropical marine faunas were largely cosmopolitan.
28 Overall, this suggests that the Famennian was marked by long-term environmental
29 changes occurring in a relatively homogeneous manner despite being punctuated by
30 several short-term events of limited faunal impact. How these trends were modulated
31 according to geographic location is investigated in this study by comparing two
32 continuous outcrops in the Montagne Noire (Col des Tribes section, France) and in Saxo-
33 Thuringia (Buschteich section, Germany). Both were located in the subtropical area
34 during this period and belonged to two former microcontinents bracketed between the
35 closing Rheic Ocean and Gondwana. Sedimentary facies, oxygen isotopes, and the
36 generic conodont composition (biofacies) were studied in a high resolution and in the
37 same rock samples. Sedimentary facies provided an estimate of water depth and oxygen

38 isotopes were used as paleotemperature proxy. Conodont biofacies were analyzed using
39 a principal component analysis, allowing the expression of the variations in the two
40 outcrops on the same axes, and a quantitative comparison with the other proxies. Sea-
41 level and temperature variations were different between the two areas. Saxo-Thuringia
42 displayed stable deep and warm conditions throughout. In contrast, the environment of
43 the Montagne Noire was shallower and cooler during the Late and latest Famennian
44 compared to the Early and Middle Famennian, congruent with the global change
45 evidenced elsewhere. The location of Saxo-Thuringia, close to the first point of closure of
46 the Rheic Ocean, might have favored active tectonics, causing a local departure from the
47 eustatic trend. The stable temperatures at BU during the Late and latest Famennian may
48 be due to the position of Saxo-Thuringia in the remnant Rheic Ocean, limiting water
49 mass exchange with open seas, and favoring the persistence of warm conditions.
50 Offshore taxa persisted later at high abundance in the Saxo-Thuringian record. The two
51 conodont biofacies records were otherwise very comparable. This suggests that other
52 factors mitigated the water depth forcing on these conodont assemblages.

53

54

55 **Keywords.** Famennian; Montagne Noire; Saxo-Thuringia; *Palmatolepis*; oxygen
56 isotopes; sedimentary facies

57

58

59 1. Introduction

60

61 The Famennian is well known for being bracketed by two of the most important
62 biological crises in the Earth's history: the Upper Kellwasser Event just before the
63 Frasnian-Famennian boundary (e.g. McGhee, 1996; Schindler, 1993; Walliser, 1996) and
64 the Hangenberg Crisis punctuating the Devonian-Carboniferous boundary (e.g. Becker et
65 al. 2016; Kaiser et al. 2008, 2015; Walliser, 1996). Many studies were devoted to these
66 crises, allowing a fine-scale characterization of the biotic and abiotic variations during
67 the hundred thousand years involved in these worldwide perturbations (Becker et al.,
68 2012; Corradini, 2003; Girard and Feist, 1997; Joachimski et al., 2009; McGhee, 1996;
69 Sandberg et al., 1988; Walliser, 1996). Environmental changes also occurred during the
70 time interval between the crises (ca. 13 Myr, Becker et al., 2012), but deserved much

71 less attention. Short-term events have nevertheless been described, with minor impact
72 on the faunas (e.g. *Annulata* Events by House, 1985; Korn, 2004; Hartenfels, 2011;
73 Hartenfels and Becker, 2017; Dasberg Crisis by Becker, 1993; Hartenfels and Becker,
74 2009; Hartenfels, 2011; Condroz Events by Becker, 1993; Becker and House, 1997). A
75 regressive trend punctuated by minor transgressive-regressive couplets has been
76 evidenced for the Famennian (Johnson et al., 1985, 1996). Global cooling inferred from
77 oxygen isotope data has been suggested for the same interval (Joachimski et al., 2004,
78 2009), an interpretation supported by independent evidence of Latest Famennian
79 glacial deposits described from South America (Caputo et al., 2008; Isaacson et al.,
80 2008). The congruence of climate cooling and a regressive trend is therefore coherent in
81 this eustatic context. Tropical and subtropical marine faunas were cosmopolitan at the
82 generic level (Feist and Becker, 1997; Korn and De Baets, 2015; Mottequin et al., 2013;
83 Spalletta et al., 2017) suggesting rather homogeneous environmental conditions and
84 efficient exchanges between the faunas. Conodonts, small, nektonic animals of chordate
85 affinities, were an abundant part of this marine fauna. Their taxonomic identification
86 provides a detailed stratigraphic framework for this period (Hartenfels, 2011; Spalletta
87 et al., 2017; Ziegler, 1962; Ziegler and Sandberg, 1984; 1990). Conodonts can also give
88 paleoenvironmental indications because conodont genera distribution was influenced
89 by several factors (Lüddecke et al., 2017), notably water depth (Sandberg, 1976; Seddon
90 and Sweet, 1971). The congruence of temporal variations in the conodont biofacies (i.e.
91 assemblage composition of the different genera) in different sections supported that the
92 Famennian was marked by long-term environmental changes that were not durably
93 perturbed by the short-term events punctuating it (Corradini, 2003; Girard et al., 2014;
94 2017).

95 This view, however, can also be the consequence of the paucity of detailed
96 records in different paleogeographic areas. Famennian paleogeography was
97 characterized by the closure of the Rheic Ocean bracketing microcontinents derived
98 from Gondwana (e.g. Franke et al., 2017; Stampfli et al., 2013) (Fig. 1). Discrepancies in
99 relative sea-level changes have been reported from these microcontinents (e.g. in the
100 Saxo-Thuringian area) and attributed to tectonic movements overprinting the global
101 eustatic trend (Girard et al., 2017). This raises the question whether the environmental
102 trends evidenced so far are of global significance, and/or whether local/regional factors

103 related to tectonics and paleogeographic changes interfered with these (presumed)
104 global trends.

105 To address these questions, we studied two recently described sections having a
106 detailed record from the Late Frasnian to the end-Famennian (Girard et al., 2014, 2017).
107 The Col des Tribes (CT) section in the Montagne Noire was part of the Armorica
108 microcontinent, whereas the Buschteich section (BU) was located on the Saxo-
109 Thuringian microplate. Hence, both sections were located on former microcontinents
110 bracketed between the closing Rheic Ocean and Gondwana (Fig. 1). Water depth and
111 approximate position relative to the shore were assessed based on the macroscopic
112 description of the sediments as well as microfacies analysis (e. g. Flügel, 2004). Despite
113 limitations due to the scarcity of preserved bioclasts in the sediments (e.g. Brett and
114 Allison, 1998), this approach provided a paleoenvironmental estimate directly based on
115 the depositional environment. Water depths derived from sedimentological analysis
116 were compared with conodont biofacies, which have been proposed to react more
117 sensitive to water-depth changes than microfacies (Lüddecke et al., 2017). Nevertheless,
118 as for any biotic record, evolutionary changes through time (changes in water depth
119 preferences, decrease or increase in response to biotic factors such as predation or
120 competition) may interfere with the paleoenvironmental signature (Belka and Wendt,
121 1992). A multivariate approach was developed to quantitatively compare the conodont
122 assemblages in the studied sections. In addition, paleotemperatures were reconstructed
123 using oxygen isotopes measured on conodont apatite.

124 A strength of this study is that the three proxies are derived from the same rock
125 samples taken at a comparable temporal resolution, allowing for detailed and
126 quantitative comparisons. The following questions are addressed: (1) Did
127 environmental changes affect similarly and at the same pace both areas, and if not, how
128 to interpret any discrepancies? (2) Did water depth and temperature covary, as
129 expected for eustatic trends during a global cooling culminating with the Devonian-
130 Carboniferous boundary glaciation (Buggisch et al. 2008; Caputo et al., 2008; Isaacson et
131 al., 2008)? (3) Was the forcing of water depth changes recorded as expected on
132 conodont biofacies? In that context, did conodont biofacies rather react to local
133 deviations from, or to globally recorded paleoenvironmental trends?

134

135 **2. Geological setting**

136 During the Late Devonian, the Col des Tribes (CT; Montagne Noire/France; Girard
137 et al., 2014) and Buschteich (BU; Thuringia/Germany; Girard et al., 2017) sections were
138 located in subtropical latitudes on different microcontinents (Fig. 1). These
139 microcontinents progressively migrated towards the equator and Laurussia during this
140 period due to the closure of the Rheic Ocean (Franke et al., 2017). The absence of
141 provincialism in benthic faunas compared to Laurussian faunas suggests that the Rheic
142 Ocean was, at that time, already reduced (Feist and Becker, 1997; Mottequin et al.,
143 2013). It has been proposed that the Saxo-Thuringia microcontinent, on which BU was
144 located, was situated in the middle of the sea between the remnant Rheic Ocean and the
145 Paleotethys (Franke et al., 2017) during the Late Frasnian (375 Ma). By the latest
146 Famennian (~360 Ma), this seaway was almost or completely closed, locating BU at the
147 margin of the remnant Rheic Ocean (Fig. 1). The Montagne Noire, including CT, was
148 located on the Armorica microcontinent which was presumably positioned further
149 towards the Paleotethys Ocean. Nevertheless, the precise location of these
150 microcontinents relative to Laurussia as well as their position relative to each other is
151 debated (e.g. Eckelmann et al. 2014; Franke et al. 2017).

152 Both sections expose Late Frasnian to Late Famennian deposits, although with a
153 gap during the earliest Famennian in BU. Their stratigraphical context has been formerly
154 described (Girard et al., 2014, 2017) using the zonation of Ziegler and Sandberg (1990);
155 and has been updated applying the zonation of Spalletta et al. (2017) in this study (Fig.
156 2). The CT section (Girard et al., 2014) is ca. 80 m thick. It consists of fine-grained
157 bioclastic limestones from the *Palmatolepis rhenana* to the *Pa. glabra pectinata*
158 conodont Zone, followed by typical reddish griottes from the *Pa. rhomboida* to the *Pa.*
159 *marginifera marginifera* Zone. Lime mudstones were deposited from the *Pa. marginifera*
160 *utahensis* to the *Pa. rugosa trachytera* Zone and are overlain by wackestones with an age
161 from the *Polygnathus styriacus* to the middle of the *Bispathodus ultimus* Zone. The
162 Famennian carbonate deposits are overlain by the Hangenberg shales. Depositional
163 environments ranged from mid to outer ramp. The BU section is ca. 35 m thick and
164 consists of lime mudstones and fine-grained turbiditic wackestones from the *Pa.*
165 *rhenana* to the *Scaphignathus velifer velifer* Zone, followed by nodular limestones of the
166 *Pa. rugosa trachytera* to the middle of the *Bispathodus ultimus* Zone and the Hangenberg
167 shales. Depositional environments ranged from distal slope to outer ramp (Girard et al.,
168 2017).

169

170 3. Materials

171 Sixty-four and forty samples were collected from the CT and BU sections,
172 respectively (Supplementary Table). Thin sections were used for microfacies analysis.
173 Conodonts were extracted by dissolving a fraction of the samples using 10% formic acid.
174 All conodonts were manually picked from the insoluble residues and determined at the
175 generic and species level. The taxonomic identification allowed establishing a detailed
176 biostratigraphic scheme. The abundance of conodonts is high to exceptionally high, with
177 about 600 platform elements per kg at CT and about 7000 platform elements per kg at
178 BU. Entire and broken platform elements representing at least half of an element were
179 counted per genus to characterize conodont biofacies in each sample (Sandberg, 1976).
180 A fraction of these conodonts was thereafter used for oxygen isotope analyses. All
181 approaches (microfacies, conodont biofacies, and oxygen isotope geochemistry) were
182 performed on the same rock sample.

183

184 4. Methods

185 4.1. Age model

186 The stratigraphy of Late Devonian deposits is mostly based on conodont
187 biostratigraphy. A revised global standard of the Famennian (Late Devonian) conodont
188 zonation has been recently published (Spalletta et al., 2017). Zonal boundaries and
189 duration are essentially identical to those of Ziegler and Sandberg (1990), which was
190 used in the Global Time Scale 2012 (Becker et al., 2012) to date in absolute ages some
191 zonal boundaries. In this study, the zonal boundaries dated in the Global Time Scale
192 2012 were used as anchor points to establish local linear regressions between absolute
193 age and depth along the sections, thus providing age estimates for each sampled level.
194 Anchor points are the basis of the following zones: *Palmatolepis triangularis*, *Pa. crepida*,
195 *Pa. rhomboidea*, *Pa. marginifera marginifera*, *Pa. rugosa trachytera*, *Polygnathus*
196 *styriacus*, *Palmatolepis gracilis expansa* (adapted to the zonation of Spalletta et al. 2017),
197 and the base of the Early *praesulcata* sensu Ziegler and Sandberg (1990).

198

199 4.2. Sedimentary facies description

200 The description of the sedimentary facies in the Col des Tribes and Buschteich
201 sections has been published by Girard et al. (2014) and Girard et al. (2017), respectively.

202 The different facies were characterized by the sedimentological and biological features
203 from outcrops as well as thin sections, allowing an interpretation of the different
204 depositional settings. For each section, this led to an ordering ('score') of the different
205 samples along a theoretical proximal-distal gradient. In order to compare BU and CT, the
206 scoring of the sedimentary facies (later on in the text: 'facies') in the two outcrops have
207 been compiled into a single scheme.

208

209 *4.3. Oxygen isotope analyses*

210 Oxygen isotope ratios of conodont apatite can be used as a paleotemperature
211 proxy (Joachimski and Buggisch, 2002; Joachimski et al., 2009; Luz et al., 1984). Twenty-
212 seven conodont samples from the Buschteich section and 26 conodont samples from the
213 Col des Tribes section have been studied for oxygen isotopes. Chemical conversion of
214 apatite bound phosphate into trisilverphosphate (Ag_3PO_4) was performed according the
215 method described in Joachimski et al. (2009). Oxygen isotope analyses were performed
216 using a TC-EA (high-temperature conversion-elemental analyzer) coupled online to a
217 ThermoFinnigan Delta V Plus mass spectrometer. 0.2 to 0.3 mg Ag_3PO_4 was weighed into
218 silver foil and transferred to the sample carousel of the TC-EA. At 1450 °C, the silver
219 phosphate is reduced and CO forms as the analyte gas (Vennemann et al., 2002). CO was
220 transferred in a helium stream through a gas chromatograph via a Conflo III interface to
221 the mass spectrometer. All values are reported in ‰ relative to V-SMOW. Samples as
222 well as standards were generally measured in triplicate. The measurements were
223 calibrated by performing a two-point calibration (Paul et al., 2007) using NBS 120c
224 ($\delta^{18}\text{O} = 21.7\text{‰}$) and a commercial Ag_3PO_4 (9.9‰). A laboratory standard was used as a
225 control standard and processed together with the samples. All standards were
226 calibrated to TU1 ($\delta^{18}\text{O} = +21.11\text{‰}$) and TU2 (+5.45‰; Vennemann et al., 2002). The
227 average oxygen isotope composition of the internationally distributed standard NBS
228 120c was measured as $+21.67 \pm 0.09$ (1 σ ; n= 5).

229

230 *4.4. Conodont biofacies*

231 Late Devonian conodont taxa were supposed to have different water depth
232 preferences (Klapper and Barrick, 1978; Seddon and Sweet, 1971). Hence, the
233 proportion of the different genera within a given assemblage was interpreted as a proxy
234 of water depth (Sandberg, 1976; Seddon and Sweet, 1971). Refined biofacies

235 interpretations based on conodont subgenera or even species have been proposed (e.g.
236 Lüddecke et al., 2017) but due to species evolution and replacement through time, this
237 approach appeared difficult to apply to the relatively long record considered in the
238 present study. During the late Frasnian to late Famennian, at least seven genera are
239 present and can provide information about depositional environments (e.g. Corradini,
240 2003; Morrow, 2000; Sandberg, 1976; Seddon and Sweet, 1971). The genera that have
241 been most clearly associated to water depth preferences are the following. (1) For deep
242 waters, *Palmatolepis* and *Bispathodus/Branmehla/Mehlina*. It should be noted that
243 whereas *Palmatolepis* is considered to be a specialist of offshore environments,
244 *Bispathodus* presents wider tolerance to water depth and/or proximity to the shore
245 (Ziegler and Sandberg 1984). (2) *Polygnathus* for intermediate water depth. (3) *Icriodus*,
246 *Scaphignathus*, and *Alternognathus* for shallow waters. Due to their low abundance and
247 similar environmental preferences, the two latter genera have been grouped for
248 biofacies representation. Hence, in this study, the following biofacies were recognized:
249 the palmatolepid biofacies, the palmatolepid-polygnathid biofacies, and the bispathodid-
250 polygnathid biofacies.

251

252 4.5. Data analysis and statistics

253 The proportion of each genus was estimated in each sampled level based on
254 counting (Girard et al., 2014, 2017). The description of these proportions corresponds to
255 the conodont biofacies analysis itself. A principal component analysis (PCA on the
256 variance-covariance matrix) was performed on these percentages to summarize the
257 variation of all genera on few main axes. This analysis also provided a representation of
258 the records of CT and BU on the same synthetic axes, allowing a direct comparison of the
259 biofacies variations in the two outcrops. The contribution of each genus percentage to
260 the axes allowed their interpretation in relation to the biofacies. The PCA was performed
261 using the R package *ade4* (Dray and Dufour, 2007). The different proxies (microfacies,
262 oxygen isotope ratios and the first axis of the PCA on the conodont percentages) were
263 compared using linear regression analysis in CT and BU separately, and in the combined
264 dataset (CT+BU). To test for a secular climate evolution, the relationship between
265 oxygen isotope values and time was tested using linear regressions in CT, BU and
266 CT+BU. In addition, this relationship was also investigated using a linear model
267 including as terms the age of the levels, the section and the interaction between the two

268 former terms. If the interaction between two terms, here age and section, is significant,
269 this means that the relationship of the dependent variable (here, $\delta^{18}\text{O}$ values) to age
270 have a different slope in the two sections. To test if $\delta^{18}\text{O}$ values were different in two
271 phases of the record, t-tests were also used. All these tests were performed under R (R
272 Core Team, 2017). An analysis of variance (ANOVA) on a linear model combining
273 microfacies and oxygen isotopes as explanatory variables was used to assess their
274 relative influence on conodont assemblages, estimated by the scores along the first axis
275 of the PCA on conodont percentages. A type II ANOVA was used, because this method is
276 invariant to ordering of the model terms and is powerful even with unbalanced datasets.
277 This test was done using the R package *ffmanova* (Langsrud and Mevik, 2012).

278

279 **5. Results**

280 *5.1. Age model*

281 The absolute ages estimated in Becker et al. (2012) for some zonal boundaries
282 served us as anchor points. A correlation with sediment thickness allowed establishing
283 an age model for each section (Fig. 2). The observed sediment thickness includes post-
284 depositional processes such as compaction, erosion, and diagenesis, that may affect the
285 estimates of accumulation rates through time and between sections. With this limitation,
286 Famennian mean accumulation rates were low in CT (5 to 7 mm/kyr⁻¹) and extremely
287 low in BU (1 to 3 mm/kyr⁻¹). Two periods of more or less constant accumulation rates
288 can be identified in BU: one from the *Pa. crepida* Zone to the *Sc. velifer velifer* Zone, and a
289 second, with even lower rates, from the *Palmatolepis rugosa trachytera* Zone to the end
290 of the Famennian. In CT, these two intervals can also be recognized, with possibly a
291 temporary acceleration of deposition during the *Pa. marginifera marginifera* and
292 *marginifera utahensis* Zones. The ages estimated for each sample were thereafter used
293 to plot the variations of the conodont assemblages and of the environmental proxies.
294 This allowed a comparison of the timing of changes in both sections.

295

296 *5.2. Sedimentary facies*

297 The sedimentary facies of BU and CT have been compiled into a single scheme.
298 Five facies types have been distinguished based on microfacies and faunal content (Fig.
299 3). The interpolated scheme is summarized below and compared to the published facies
300 at CT (Girard et al., 2014) and BU (Girard et al., 2017). Details are provided in the Supp.

301 Table 1. Based on these facies characteristics, the temporal variation in the depositional
 302 setting can be reconstructed. Note that all depositional environments are relatively
 303 deep, and correspond to the deepest environments found on the shelf, and that the
 304 terms 'shallow' and 'deep' are used in the context of relative shallowing or deepening. At
 305 BU only minor variations can be observed (Fig. 4A). The depositional environment,
 306 mostly corresponding to Facies 2, remained relatively deep throughout the record.
 307 Intervals with the even deeper Facies 1 can be identified during the Late Frasnian, the
 308 *Pa. crepida and termini* Zones, the *Pa. marginifera marginifera* Zone, the *Sc. velifer velifer*
 309 Zone, and the top of *Bispathodus ultimus* Zone. The CT section shows evidence for more
 310 important changes in water depth. A first shallowing episode occurred during the latest
 311 Frasnian and earliest Famennian, followed by a second, shallower episode during the *Pa.*
 312 *gracilis gracilis* and the *Pa. marginifera marginifera* Zones. From the top of the
 313 *Pseudopolygnathus granulosus* Zone to the end of the Famennian, conditions were
 314 constantly shallower than during the two former episodes. These shallowing trends are
 315 separated by two deepening episodes, from the *Pa. minuta minuta* to the *Pa. rhomboidea*
 316 Zone and from the *Pa. marginifera marginifera* to the *Pseudopolygnathus granulosus*
 317 Zone.

318

319 5.3. Oxygen isotopes

320 Oxygen isotope ratios measured on conodont apatite from CT are between +17.1
 321 and +17.7‰ from the end Frasnian to the *Pa. crepida* zone (Fig. 4B). Values thereafter
 322 more or less gradually increase to values around 18‰ in the *Pa. marginifera utahensis*
 323 Zone. From the *Sc. velifer velifer* to the *Pa. gracilis expansa*, $\delta^{18}\text{O}$ increases to values
 324 above +19‰. A slight decrease is observed to the end of the Famennian. Oxygen isotope
 325 values of conodont apatite from BU are generally higher than values observed at CT.
 326 $\delta^{18}\text{O}$ values range from +16.4 to +16.9 ‰ from the end Frasnian to the *Pa. crepida* zone.
 327 From a minimum of +16.4 ‰ at the base of the *Pa. crepida* Zone, a trend to higher
 328 values occurs up to the *Pa. marginifera marginifera* Zone, reaching $\delta^{18}\text{O}$ values of +17.8
 329 ‰. A brief decrease marks the first part of the *Pa. marginifera utahensis* Zone, with $\delta^{18}\text{O}$
 330 values of around +16.7 ‰. Thereafter, up to the end of the Famennian, $\delta^{18}\text{O}$ values
 331 remain close to +17.5 ‰.

332 The offset in $\delta^{18}\text{O}$ between the two sections is relatively small (+0.5 to +1‰) from the
 333 *Pa. crepida* Zone to *Pa. marginifera utahensis* Zone, but increases after the *Sc. velifer*
 334 *velifer* Zone (+1 to +1.5 ‰). This difference in $\delta^{18}\text{O}$ translates into +6 to +6.5°C cooler
 335 temperatures in CT in case the offset is solely explained by temperature.

336

337 5.4. Conodont biofacies

338 The conodont biofacies follow overall comparable trends in both sections (Fig. 5;
 339 Supp. Table 1), sharing a dominance of *Palmatolepis* for most of the time up to a
 340 maximum at the base of the *Pa. marginifera marginifera* Zone (up to more than 95% of
 341 the assemblage), followed by a progressive decrease towards the end Famennian. This
 342 decrease of *Palmatolepis* was compensated almost exclusively by a rise of *Bispathodus* in
 343 CT and by a rise of both *Polygnathus* and *Bispathodus* in BU. The Frasnian assemblages
 344 were complemented by the occurrence of other genera such as *Polygnathus* and
 345 *Ancyrodella*. The *Pa. triangularis* to *Pa. minuta minuta* Zones, which are missing in BU,
 346 were marked by an increase in the abundance of *Icriodus* in CT. Another maximum in the
 347 abundance of *Icriodus* in CT is recognized in the *Pa. glabra prima* Zone. Except for the *Pa.*
 348 *crepida* Zone, *Icriodus* was rare in BU. In CT, a short-term rise of
 349 *Scaphignathus/Alternognathus* occurred around the *Ps. granulosus* Zone. A similar but
 350 more discrete rise is present at the base of the *Pa. rugosa trachytera* Zone in BU.

351

352 5.5. Multivariate analysis of the conodont taxa abundances

353 The principal component analysis performed on the proportions of the different
 354 genera allowed summarizing the biofacies variations on one main axis (PC1) expressing
 355 more than 75% of the total variance. The record of the two sections CT and BU can be
 356 directly compared on these axes. The contribution of the variables (here, the
 357 percentages of the different genera) to the axes (Fig. 6A) shows that positive values
 358 along the first axis correspond to a high proportion of *Palmatolepis* whereas negative
 359 values correspond to a high proportion of *Bispathodus*. Variations along the PC1 axis
 360 thus correspond to the replacement of *Palmatolepis* by *Bispathodus*. The second axis
 361 represents only less than 20% of variance, and mostly corresponds to variations in the
 362 proportion of *Polygnathus*. Other genera contribute very little to the two main axes, due
 363 to their rare occurrence in the records.

364 Representing the different levels in the first principal plane of this PCA allows for
 365 a comparison of BU and CT conodont biofacies variations (Fig. 6B-I). Most of the time,
 366 the range of values covered by samples from the two sections largely overlaps. The
 367 oldest samples (mostly Frasnian) are characterized by a peculiar diagonal distribution
 368 (Fig. 6B). Their shift in the PCA space compared to Famennian samples is due to the
 369 occurrence of genera such as *Ancyrodella* that went extinct during the Frasnian -
 370 Famennian crisis. Early Famennian levels of both sections are tightly clustered, sharing
 371 extreme positive values along the first axis, due to the overwhelming dominance of
 372 *Palmatolepis*.

373 In CT, a shift towards negative PC1 values is launched between the *Pa.*
 374 *marginifera marginifera* and *Pa. marginifera utahensis* Zones (Fig. 4C, 6E),
 375 corresponding to the onset of the decrease in the abundance of *Palmatolepis* (Fig. 5).
 376 This shift went on to reach extreme negative PC1 values as early as the *Po. styriacus*
 377 Zone (Fig. 6G, H). This change started more or less at the same time at BU, but it did not
 378 occur in a consistent manner for a while. Only towards the end of the studied interval,
 379 during the *Bispathodus ultimus* Zone, PC1 values in BU reach a range similar to the one
 380 observed in CT (Fig. 6I). This corresponded to the final decrease of *Palmatolepis* at BU,
 381 close before its extinction near the Devonian-Carboniferous boundary (Fig. 5). The
 382 consequence of this delay in the decrease of *Palmatolepis* at BU was a temporary offset
 383 between the two records of conodont genera proportions, starting during the *Ps.*
 384 *granulosus* Zone and persisting until the base of the *Bi. ultimus* Zone (Fig. 4C).

385

386 5.6. Comparison of paleoenvironmental proxies and conodont biofacies

387 As a first step, we compared the different proxies (Table 2). Facies, oxygen
 388 isotope ratios, and the first axis of the principal component analysis on the conodont
 389 percentages (later on mentioned as conodont PC1) are all significantly correlated when
 390 considering the total dataset (CT+BU). In contrast, none of the correlations is significant
 391 when considering BU. At CT, conodont PC1 is significantly correlated to facies and $\delta^{18}\text{O}$,
 392 but the two latter variables are not correlated.

393 The variation in the oxygen isotope ratios shows a significant secular trend, the
 394 relationship of $\delta^{18}\text{O}$ and age being significant in the CT, BU and CT+BU datasets.
 395 In the linear model investigating the variation of $\delta^{18}\text{O}$ depending on age in the two
 396 sections, the interaction term between $\delta^{18}\text{O}$ and age is not significant. This means that

397 the slope of the regression is the same in the two sections. While the two sections
 398 display a similar increase in $\delta^{18}\text{O}$ when considering the whole record, from the end
 399 Frasnian to the Late Famennian, the records of CT and BU do not follow a similar pattern
 400 after the *Pa. marginifera utahensis* Zone (Fig. 4B). The oxygen isotope ratios increase in
 401 CT but remain stable in BU. To test for such a discrepancy between the records of the
 402 two sections, we performed t-tests between oxygen isotope values of the period
 403 preceding and following the apparent shift in CT. The difference in $\delta^{18}\text{O}$ is indeed
 404 statistically significant in CT (t-test [from *Pa. rhomboidea* to *Sc. velifer velifer*, n = 8] vs.
 405 [from *Pa. rugosa trachytera* to *Bi. ultimus*, n = 7], P = 0.0026). In contrast, the $\delta^{18}\text{O}$ values
 406 of the same periods do not differ in BU (t-test [n = 6 and 11], P = 0.3443).

407 Finally, to investigate whether $\delta^{18}\text{O}$ or facies better explains the variation of the
 408 conodont genera, linear models with conodont PC1 as dependent variable, and $\delta^{18}\text{O}$ and
 409 facies as independent factors were considered (Table 3). The interaction term between
 410 both factors ($\delta^{18}\text{O}$ and facies) is weak (p = 0.0311 for CT+BU) or not significant (for CT
 411 and BU separately). This term was therefore discarded from the models. Facies and $\delta^{18}\text{O}$
 412 are significant explanatory variables of conodont biofacies when considering CT and BU
 413 together, and CT alone. Facies explains more than three times more variance than $\delta^{18}\text{O}$
 414 in both cases. None has significant effect in BU.

415

416 6. Discussion

417 Our detailed oxygen isotope records generally show an increase in $\delta^{18}\text{O}$ in both
 418 sections from the end Frasnian to end Famennian, coherent with described global
 419 cooling during this time interval (Joachimski et al., 2009). However, in details, the two
 420 records show different temperature variations from the *Pa. rugosa trachytera* Zone to
 421 end Famennian. While temperature remained more or less stable throughout the
 422 Famennian in the BU section (Saxo-Thuringia), it decreased in the CT section (Montagne
 423 Noire) towards *Sc. velifer velifer* Zone. This difference in $\delta^{18}\text{O}$ between CT and BU is
 424 mirrored by different sea-level variations in CT and BU, as pointed out by facies
 425 description. Given these differences between the paleoenvironmental settings of the two
 426 areas, conodont biofacies delivered remarkably similar records, questioning the role of
 427 the paleoenvironmental forcing on conodont assemblages.

428

429 *6.1. Paleotemperature variations: a global trend mitigated by paleogeography?*

430 A global temperature trend has been sketched for the Late Devonian (McGhee,
431 2013), based on variations in $\delta^{18}\text{O}$ of conodont apatite (Joachimski et al., 2009). This
432 composite record showed a rapid succession of cooling and warming pulses around the
433 Frasnian-Famennian boundary (Balter et al., 2008; Joachimski and Buggisch, 2002;
434 Huang et al. 2018). After a warm period during the *triangularis* Zone, a progressive long-
435 term cooling was proposed for the rest of the Famennian (Joachimski et al., 2009),
436 culminating into a period with stable ice caps during the early Carboniferous (Buggisch
437 et al. 2008). As for some other oxygen isotope studies in the Paleozoic, our isotope
438 records are based on conodont apatite, thus tracing the environment where the
439 conodont lived. Furthermore, all analyses were performed on the same genus,
440 *Palmatolepis*, avoiding the problem that different oxygen isotope values in the two
441 sections may be due to analyses on genera with different habitat preferences. Our
442 results support a long-term cooling, since the two sections displayed a parallel increase
443 in the oxygen isotope ratio from the end Frasnian to end Famennian, although more
444 pronounced in CT than in BU. An offset, however, exists between the records of the two
445 sections, with BU constantly showing lower $\delta^{18}\text{O}$ values than CT. Based on the
446 paleogeographic reconstruction (Fig. 1), BU and CT were both in the subtropical zone.
447 The constant offset between the two records can thus hardly be explained by a
448 latitudinal difference. Possibly, CT being positioned further towards the Paleotethys
449 (Franke et al., 2017), it might have been more exposed to the colder water masses of the
450 open Paleotethys Ocean and Paleo-Adria epicontinental sea.

451 Beyond the cooling trend registered in both sections from the *Pa. crepida* to *Pa.*
452 *marginifera* Zone, the oxygen isotope records from BU and CT show differing
453 trends after the *Pa. marginifera utahensis* Zone. This pattern is also seen in other
454 sections studied by Joachimski et al. (2009). For example, in the La Serre section
455 (Montagne Noire) an increase in $\delta^{18}\text{O}$ is reported between the *marginifera marginifera*
456 and *Sc. velifer velifer* Zones, similar and synchronous to the one documented in CT. In
457 contrast in the Kahlleite section (Saxo-Thuringian area) $\delta^{18}\text{O}$ is relatively stable as in BU
458 (Fig. 4). The difference in the $\delta^{18}\text{O}$ records of the BU and CT sections after the *Pa.*
459 *marginifera utahensis* Zone is thus confirmed at the regional scale, suggesting that the
460 paleogeographic position of the two microcontinents may have controlled the
461 temperature changes.

462 Paleogeographic reconstructions suggest that Saxo-Thuringia was located close
463 to the first zone of closure of the Rheic Ocean (Franke et al., 2017). As the closure of the
464 Rheic Ocean progressed during the Famennian, the area might have been influenced by
465 a relative restriction of the water masses exchanges between the Rheic Ocean and the
466 Paleotethys Ocean. The upper water column temperatures might have been warmer
467 than in the open sea, as e.g. nowadays in the Caribbean Sea, the Persian Gulf, or the
468 eastern Mediterranean (see for instance Schlitzer, 2006; Schmidt et al., 2016),
469 dampening the effects of the global cooling, especially in a subtropical area. In contrast,
470 the CT section and more generally the Armorica area, being opened towards the
471 Paleotethys Ocean, would have been exposed to the Paleotethys water circulation and
472 global temperature trends, as established by Joachimski et al. (2009). This
473 interpretation is corroborated by the fact that Late Famennian $\delta^{18}\text{O}$ values recorded in
474 the Carnic Alps (Paleo-Adria, Fig. 1; *Pa. gracilis expansa* and *Bi. ultimus* Zones: $\sim 18,3$ ‰;
475 Kaiser et al., 2006, 2008), and hence also in an environment open towards the
476 Paleotethys (Paleo-Adria on Fig. 1), were closer to those recorded at CT than at BU.

477

478 6.2. Water depth variations, combination of eustatic trends and local tectonics

479 Sea-level variations correspond to a high-stand during the end of the Frasnian,
480 followed by a progressive sea-level fall during the Famennian (Haq and Schutter, 2008;
481 Johnson et al., 1985, 1996; Sandberg et al., 2002). These variations appear to have
482 occurred world-wide, thus pointing to eustatic trends (Johnson et al., 1985, 1996). In
483 this context, a decrease in water depth should coincide with increasing ice volume, a
484 glacio-eustatic sea-level fall and a temperature decrease. In the CT section, a regressive
485 trend and a cooling are indeed registered, but they do not occur in parallel with the
486 shallowing clearly postponing the shift towards colder temperature. Another
487 discrepancy with the expectation is that both the temperature and water depth decrease
488 do not seem to have occurred in a progressive manner, but rather abruptly. Possibly,
489 paleogeographic and/or tectonic events might have temporarily mitigated the
490 expression of the long-term trend in CT. Water depth variations in BU do not follow this
491 global trend. In BU, the depositional environment remained deep throughout the
492 Famennian, and tectonic activity has been invoked to explain this discrepancy (Girard et
493 al., 2017). The paleogeographic position of Saxo-Thuringia, close to Baltica and hence

494 one of the first microcontinent to collide with it, matches well with active tectonics
495 causing a local departure from the eustatic trend.

496

497 *6.3. Congruent variations of the conodont assemblages despite discrepant*
498 *paleoenvironmental settings*

499 In contrast to the different patterns of temperature variation after the *Pa.*
500 *marginifera utahensis* Zone, and differences in water depth records in CT and BU, trends
501 in conodont biofacies are quite comparable. Both sections reflect a dominance of
502 *Palmatolepis* for most of the Famennian with a decline starting in the *Pa. marginifera*
503 *marginifera* Zone. If the difference between the environments at CT and BU had any
504 impact on the conodont assemblages, it was only minor and corresponded to a transient
505 offset between the two conodont records. However, conodont biofacies are advocated to
506 be mostly driven by water depth variations, due to the habitat preferences of the
507 different conodont genera (Sandberg, 1976; Seddon and Sweet, 1971). Initially, two
508 ecological models, i.e. depth stratification vs. lateral segregation, were proposed
509 (Klapper and Barrick, 1978; Seddon and Sweet, 1971). The depth-stratification model
510 implies that specific conodont taxa inhabited different depth zones within the water
511 column, whilst the lateral segregation model proposes that bottom-dwelling taxa were
512 dominantly controlled by habitat properties near the sediment–water interface. The
513 abundant occurrence of conodonts during anoxic events precludes a benthic or
514 nektobenthic lifestyle. During the Frasnian and the Famennian, genera supposed to have
515 “shallow preferences” (e.g. *Icriodus*) and “preferences for deep environments” (e.g.
516 *Palmatolepis*) have been shown to share similar oxygen isotope signatures, suggesting
517 that they were living in the same water-mass (Joachimski et al., 2009). This supports the
518 interpretation that all genera were at that time living close to the surface, but occupying
519 proximal or distal locations. The higher proportion of the offshore surface dweller genus
520 *Palmatolepis* in the sediments from BU than from CT is coherent with the more off-shore
521 depositional setting in BU. The decrease of the genus *Palmatolepis* after the *Pa.*
522 *marginifera marginifera* Zone is also coherent with the regressive trend characterizing
523 the Famennian. Possibly, before the *Sc. velifer velifer* Zone, water depth was constantly
524 deep enough to favor the dominance of this offshore surface dweller genus. However, if
525 a direct forcing of water depth on conodont distribution is assumed, conodont biofacies
526 at BU should have been relatively stable through time, and depart more clearly from the

527 trend observed at CT. This suggests that the response of conodont assemblages to water
528 depth was mitigated by other factors. Possibly, the eustatic regressive trend was
529 disadvantageous to the offshore surface dweller genus *Palmatolepis* at a worldwide
530 scale, triggering its global decline. Ultimately, it would have even declined in constantly
531 deep environments such as BU, although with a time lag suggesting that it temporarily
532 found there a refuge of favorable environments.

533

534 *6.4. Relationship between the different paleoenvironmental proxies*

535 The three paleoenvironmental proxies considered here (sedimentary facies,
536 oxygen isotopes, and conodont biofacies) are potentially interrelated: oxygen isotopes
537 are temperature proxies; facies traces water depth and distance to the shore, related to
538 temperature trends through eustatic variations; and conodont biofacies are interpreted
539 as related to water depth due to habitat preferences of the different conodont genera
540 along a proximal-distal gradient in the surface waters. No relationship between these
541 proxies is evident in BU, but this absence of a significant correlation is probably due to
542 the reduced range of variation in the oxygen isotope ratios and facies observed in this
543 section. Oxygen isotopes and facies are correlated when considering the total data set.
544 However, conodont PC1 displays a stronger relationship with oxygen isotopes on the
545 one hand, and with facies on the other hand, than oxygen isotopes with facies: the
546 percentage of variance explained is larger, leading to significant relationships in CT as
547 well (Table 2). Considering the percentage of variance explained, facies furthermore
548 appears as a better explanatory variable for conodont variations than $\delta^{18}\text{O}$. The
549 sedimentary facies trace directly the depth of the depositional environment but the
550 relevance of this approach has been discussed due to the paucity of preserved biotas in
551 old sediments (e.g. see Flügel, 2004; Lüddecke et al., 2017). The correlation evidenced
552 between facies and conodont biofacies is nevertheless coherent with the interpretation
553 of conodont genera distribution being controlled by water depth, along a proximal-distal
554 gradient (Klapper and Barrick, 1978). The fact that conodont biofacies respond earlier
555 and more progressively to the global regressive trend may be due to the fact that CT and
556 BU being located in outer shelf environments, the decrease in water depth should be
557 important enough to cause a change in the facies.

558

559 *6.5. Paleogeography and paleoenvironment: a complex interplay*

560 Many studies focused on global environmental trends in the Devonian (e.g.
561 Godd ris and Joachimski, 2004; Haq and Schutter, 2008; Miller et al., 2005; Sandberg et
562 al., 1988; Wilson and Norris, 2001), especially during the Late Devonian for which
563 environmental conditions have been suggested to be homogeneous within the
564 subtropical zone, and the marine faunas to be cosmopolitan. However, our results, based
565 on two detailed 13 My long records, indicated different paleoenvironmental changes in
566 BU and CT. After the end of the *Pa. marginifera utahensis* Zone, the cooling and the
567 regressive trend found little expression in BU compared to CT, but these differences are
568 only weakly mirrored in the conodont assemblages. The differences in the temperature
569 records of CT and BU are not only observed in the two studied sections, but registered
570 as well in two other sections (Kahlleite and La Serre) from the Saxo-Thuringian and
571 Montagne Noire areas (Joachimski et al., 2009), respectively. We propose that the
572 deviation of the BU record from what we interpret as the global trend may be attributed
573 to the paleogeography of the Saxo-Thuringian area, where a progressive restriction of
574 water-mass exchange possibly accompanied the closing of the seaway between the
575 remnant Rheic and Paleotethys oceans. This restricted paleogeography together with a
576 subtropical location might have favored the persistence of warm conditions in the sea-
577 waters where conodonts lived despite the onset of global cooling. Such setting should
578 also have been prone to active tectonics overprinting the eustatic trend. Not mutually
579 exclusive, the closure of the Rheic Ocean itself might have contributed to the global
580 climate change, by interrupting the circum-equatorial circulation (see for instance for
581 the closure of the Panama Isthmus: Bartoli et al., 2005 and Haug and Tiedemann, 1998),
582 but this remains speculative and challenges further studies.

583 Increasing the geographic coverage of a multi-proxy approach, such as the one
584 outlined here, may thus provide relevant information to better constrain
585 paleogeographic reconstructions characterized by a complex distribution of land and
586 water masses, as e.g. in the Late Devonian. This key step will contribute to a better
587 understanding of the complex interplay between paleogeography, climate, and biotic
588 response and go beyond the tempting, but misleading, view of global trends affecting the
589 different regions in a relatively homogeneous manner.

590

591 **7. Conclusions**

592 This study presents a detailed comparison of two Famennian successions in the
593 Montagne Noire (France) and Saxo-Thuringia (Germany). During the Famennian, both
594 areas were located in the subtropical realm and were part of two microcontinents
595 bracketed between the remnant Rheic Ocean and Gondwana. Based on the same rock
596 samples, paleotemperatures were estimated using oxygen isotopes of conodont apatite,
597 depositional environments were assessed based on sedimentary facies, and the
598 response of conodont assemblages was evaluated using conodont biofacies. Applying a
599 principal component analysis to biofacies data provided a synthetic axis summarizing
600 the biofacies variations along the two sections. This allowed for a quantitative
601 comparison of the biofacies records with paleoenvironmental proxies.

602 During the Famennian, both the Montagne Noire and Saxo-Thuringia display a
603 parallel increase in the oxygen isotope ratios translating into long-term cooling.
604 However, during the Late Famennian, temperatures remained stable in Saxo-Thuringia,
605 leading to a temperature offset compared to the Montagne Noire record. The Late and
606 latest Famennian are also characterized by a regressive trend which was found to be
607 well expressed in the sedimentary facies in the Montagne Noire, but not in Saxo-
608 Thuringia, where the depositional environment remained deep throughout. Despite
609 these environmental differences, conodont biofacies were rather comparable in the
610 Montagne Noire and Saxo-Thuringia. A temporary offset however suggested that
611 *Palmatolepis*, the typical off-shore surface dwelling taxon, was abundant for a longer
612 time period in the deep Saxo-Thuringian environment. The environmental differences
613 between the two areas are tentatively explained by their paleogeographic location. The
614 Saxo-Thuringian microplate is interpreted as located close to the point of first closure of
615 the Rheic Ocean and thus might have been influenced by active tectonism and a
616 restricted water mass exchange, blurring the impact of the long-term trends in this
617 setting.

618

619 **Acknowledgments**

620 We thank D. Delmas and C. Nevado (Lyon, France) who produced the thin-sections and
621 Raimund Feist (Montpellier, France), Dieter Weyer (Berlin, Germany) and Konrad
622 Bartzsch (Saafeld, Germany) for their contribution during field trips. The research was
623 supported by the ANR Project ECODEV (ANR-13-BSV7-005). This is publication ISEM
624 2018-XXX.

625
626
627

References

- 628 Balter, V., Renaud, S., Girard, C., Joachimski, M.M., 2008. Record of climate-driven
629 morphological changes in 376 Ma Devonian fossils. *Geology* 36, 907-910.
- 630 Bartoli, G., Sarnthein, M., Weinelt, M., Erlenkeuser, H., Garbe-Schönberg, C.-D., Lea, D.W.,
631 2005. Stable isotope analysis and temperature reconstruction data from DSDP Hole 94-
632 609B and ODP Hole 162-984B, Supplement to: Bartoli, G. et al. (2005): Final closure of
633 Panama and the onset of northern hemisphere glaciation. *Earth Planet. Sci. Lett.*, 237,
634 33-44, <https://doi.org/10.1016/j.epsl.2005.06.020>. PANGAEA.
- 635 Becker, R.T., 1993. Anoxia, eustatic changes, and upper Devonian to lowermost
636 Carboniferous global ammonoid diversity, in: House, M.R. (Ed.), *The Ammonoidea:
637 Environment, Ecology, and Evolutionary Change*. Systematics Association Special
638 Volume, Oxford, pp. 115-163.
- 639 Becker, R.T., Gradstein, F.M., Hammer, O., 2012. The Devonian Period, in: Gradstein, F.M.,
640 Ogg, J.G., Schmitz, M.D., Ogg, G.M. (Eds.), *The Geologic Time Scale 2012*. Elsevier,
641 Oxford, pp. 559-602.
- 642 Becker, R.T., House, M.R., 1997. Sea-level changes in the Upper Devonian of the Canning
643 Basin, Western Australia. *Cour. Forsch.-Inst. Senckenberg* 199, 126-146.
- 644 Becker, R.T., Kaiser, S.I., Aretz, M., 2016. Review of chrono-, litho- and biostratigraphy
645 across the global Hangenberg Crisis and Devonian–Carboniferous Boundary, in:
646 Becker, R.T., Koenigshof, P., Brett, C.E. (Eds.), *Devonian Climate, Sea Level and
647 Evolutionary Events*. The Geological Society of London, London, 423, 355-386.
- 648 Belka, Z., Wendt, J., 1992. Conodont biofacies patterns in the Kellwasser Facies (upper
649 Frasnian/lower Famennian) of the eastern Anti-Atlas, Morocco. *Palaeogeogr.
650 Palaeoclimatol. Palaeoecol.* 91, 143-173.
- 651 Brett, C., Allison, P.A., 1998. Paleontological Approaches to the Environmental
652 Interpretation of Marine Mudrocks, in: Schieber, Zimmerle, Sethi (Eds.), *Shales and
653 Mudstones*. E Schweizerbartsche Verlagsbuchandlung (Nagel u. Obermiller), Stuttgart,
654 pp. 301-349.
- 655 Buggisch, W., Joachimski, M. M., Sevastopulo, G., Morrow, J.R. 2008. Mississippian $\delta^{13}\text{C}_{\text{carb}}$
656 and conodont apatite $\delta^{18}\text{O}$ records — Their relation to the Late Palaeozoic Glaciation,
657 *Palaeogeogr. Palaeoclimatol. Palaeoecol.* 268(3-4), 273-292, doi:
658 [doi:10.1016/j.palaeo.2008.03.043](https://doi.org/10.1016/j.palaeo.2008.03.043).

- 659 Caputo, M.V., Melo, J.H.G., Streef, M., Isbell, J.L., 2008. Late Devonian and Early
660 Carboniferous glacial records of South America, in: Fielding, C.R., Frank, T.D., Isbell, J.L.
661 (Eds.), The Geological Society of America, Special Paper. Geol. Soc. America, pp. 161-
662 173.
- 663 Corradini, C., 2003. Late Devonian (Famennian) conodonts from the Corona Mizziu
664 Sections near Villasalto (Sardinia, Italy). *Palaeontographia Italica* 89, 65-116.
- 665 Dray, S., Dufour, A.-B., 2007. The ade4 package: implementing the duality diagram for
666 ecologists. *J. Stat. Softw* 22, 1-20.
- 667 Eckelmann, K., Nesbor, H.-D., Königshof, P., Linnemann, U., Hofmann, M., Lange, J.-M.,
668 Sagawe, A., 2014. Plate interactions of Laurussia and Gondwana during the formation
669 of Pangaea — Constraints from U–Pb LA–SF–ICP–MS detrital zircon ages of Devonian
670 and Early Carboniferous siliciclastics of the Rhenohercynian zone, Central European
671 Variscides. *Gondwana Research* 25, 1484-1500.
- 672 Feist, R., Becker, R.T., 1997. Discovery of Famennian trilobites in Australia (Late
673 Devonian, Canning Basin, NW Australia). *Geobios M.S.* 20, 231-242.
- 674 Flügel, E., 2004. *Microfacies of carbonate rocks. Analysis, Interpretation and Application.*
675 Springer Verlag, Berlin, Heidelberg, New York.
- 676 Franke, W., Cocks, L.R.M., Torsvik, T.H., 2017. The Palaeozoic Variscan oceans revisited.
677 *Gondwana Res.* 48, 257-284.
- 678 Girard, C., Feist, R., 1997. Eustatic trends in conodont diversity across the
679 Frasnian/Famennian boundary in the stratotype area, Montagne Noire, France. *Lethaia*
680 29, 329-337.
- 681 Girard, C., Cornée, J.-J., Corradini, C., Fravallo, A., Feist, R., 2014. Palaeoenvironmental
682 changes at Col des Tribes (Montagne Noire, France), a reference section for the
683 Famennian of north Gondwana-related areas. *Geol. Mag.* 151, 864-884.
- 684 Girard, C., Cornée, J.-J., Charruault, A.-L., Corradini, C., Weyer, D., Bartzsch, K., Joachimski,
685 M.M., Feist, R., 2017. Conodont biostratigraphy and palaeoenvironmental trends during
686 the Famennian (Late Devonian) in the Thuringian Buschteich section (Germany).
687 *Newsl. Stratigr.* 50, 71-89.
- 688 Goddérís, Y., Joachimski, M.M., 2004. Global change in the Late Devonian: modelling the
689 Frasnian-Famennian short-term carbon isotope excursions. *Palaeogeogr.*
690 *Palaeoclimatol. Palaeoecol.* 202, 309-329.

- 691 Haq, B.U., Schutter, S.R., 2008. A chronology of Paleozoic sea-level changes. *Science* 322,
692 64-68.
- 693 Hartenfels, S., 2011. Die globalen Annulata-Events und die Dasberg-Krise (Famennium,
694 Oberdevon) in Europa und Nord-Afrika – hochauflösende Conodonten-Stratigraphie,
695 Karbonat-Mikrofazies, Paläoökologie und Paläodiversität. *Münstersche Forschungen*
696 *zur Geologie und Paläontologie, Paleontologia e Stratigrafia* 115, 141-158.
- 697 Hartenfels, S., Becker, R.T., 2009. Timing of the global Dasberg Crisis – implications for
698 Famennian eustasy and chronostratigraphy. *Palaeontographica Americana* 63, 71-97.
- 699 Hartenfels, S., Becker, R.T. 2017. The global Annulata Events: review and new data from
700 the Rheris Basin (northern Tafilalt) of SE Morocco, in: Becker, R.T., Koenigshof, P.,
701 Brett, C. (Eds.), *Devonian Climate, Sea Level and Evolutionary Events*. Geological
702 Society, London, Special Publications 423, <http://doi.org/10.1144/SP423.1>.
- 703 Haug, G.H., Tiedemann, R., 1998. Stable carbon and oxygen isotope ratios of *Cibicidoides*
704 *wuellerstorfi*, and CaCO₃ and sand content of ODP Hole 165-999A, Supplement to:
705 Haug, GH; Tiedemann, R (1998): Effect of the formation of the Isthmus of Panama on
706 Atlantic Ocean thermohaline circulation. *Nature*, 393, 673-676,
707 <https://doi.org/10.1038/31447>. PANGAEA.
- 708 House, M.R., 1985. Correlation of mid-Palaeozoic ammonoid evolutionary events with
709 global sedimentary perturbations. *Nature* 313, 17-22.
- 710 Huang, C., Joachimski, M.M., Gong, Y., 2018. Did climate changes trigger the Late
711 Devonian Kellwasser crisis? Evidence from a high-resolution $\delta^{18}\text{O}_{\text{PO}_4}$ record from South
712 China. *Earth Planet. Sci. Letters* 495, 174-184.
- 713 Isaacson, P.E., Díaz-Martinez, E., Grader, G.W., Kalvoda, J., Babek, O., Devuyt, F.X., 2008.
714 Late Devonian-earliest Mississippian glaciation in Gondwanaland and its
715 biogeographic consequences. *Palaeogeogr. Palaeoclimatol. Palaeoecol.* 268, 126-142.
- 716 Joachimski, M., Buggisch, W., 2002. Conodont apatite $\delta^{18}\text{O}$ signatures indicate climatic
717 cooling as a trigger of the Late Devonian mass extinction. *Geology* 30, 711-714.
- 718 Joachimski, M.M., van Geldern, R., Breisig, S., Buggisch, W., Day, J., 2004. Oxygen isotope
719 evolution of biogenic calcite and apatite during the Middle and Late Devonian. *Int. J.*
720 *Earth Sci* 93, 542-553.
- 721 Joachimski, M.M., Breisig, S., Buggisch, W., Talent, J.A., Mawson, R., Gereke, M., Morrow,
722 J.R., Day, J., Weddige, K., 2009. Devonian climate and reef evolution: Insights from
723 oxygen isotopes in apatite. *Earth Planet. Sci. Lett.* 284, 599-609.

- 724 Johnson, J.G., Klapper, G., Sandberg, C.A., 1985. Devonian eustatic fluctuations in
725 Euramerica. *Geol. Soc. Am. Bull.* 96, 567-587.
- 726 Johnson, J.G., Klapper, G., Elrick, M., 1996. Devonian transgressive-regressive cycles and
727 biostratigraphy, Northern Antelope Range, Nevada: establishment of reference
728 horizons for global cycles. *Palaaios* 11, 3-14.
- 729 Kaiser, S.I., Steuber, T., Becker, R.T., Joachimski, M.M., 2006. Geochemical evidence for
730 major environmental change at the Devonian-Carboniferous boundary in the Carnic
731 Alps and the Rhenish Massif. *Palaeogeogr. Palaeoclimatol. Palaeoecol.* 240, 146-160.
- 732 Kaiser, S.I., Steuber, T., Becker, R.T., 2008. Environmental change during the Late
733 Famennian and Early Tournaisian (Late Devonian–Early Carboniferous): implications
734 from stable isotopes and conodont biofacies in southern Europe. *Geol. J.* 43, 241-260.
- 735 Kaiser, S.I., Aretz, M., Becker, R.T., 2015. The global Hangenberg Crisis (Devonian-
736 Carboniferous transition): a review of a first order mass extinction, in: Becker, R.T.,
737 Königshof, P., Brett, C.E. (Eds.), *Devonian climate, sea level and evolutionary events.*
738 *Geol. Soc. Spec. Publ.*, London 423, 387-437.
- 739 Klapper, G., Barrick, J.E., 1978. Conodont ecology: pelagic versus benthic. *Lethaia* 11, 15-
740 23.
- 741 Korn, D., 2004. The mid-Famennian ammonoid succession in the Rhenish Mountains: the
742 "*annulata* Event" reconsidered. *Geological Quarterly* 48, 245-252.
- 743 Korn, D., De Baets, K., 2015. Biogeography of Paleozoic ammonoids, in: Klug, C., Korn, D.,
744 De Baets, K., Kruta, I., Mapes, R.H. (Eds.), *Ammonoid Paleobiology: From*
745 *macroevolution to paleogeography.* Springer, New York, pp. 299-328.
- 746 Langsrud, Ø., Mevik, B.-H., 2012. *ffmanova: Fifty-fifty MANOVA*, [https://CRAN.R-](https://CRAN.R-project.org/package=ffmanova)
747 [project.org/package=ffmanova](https://CRAN.R-project.org/package=ffmanova).
- 748 Lüddecke, F., Hartenfels, S., Becker, R.T., 2017. Conodont biofacies of a monotonous
749 middle Famennian pelagic carbonate succession (Upper Ballberg Quarry, northern
750 Rhenish Massif). *Palaeobio. Palaeoenv.* 97, 591–613.
- 751 Luz, B., Kolodny, Y., Kovak, J., 1984. Oxygen isotope variations in phosphate of biogenic
752 apatites, III. Conodonts. *Earth Planet. Sci. Lett.* 69, 255-262.
- 753 McGhee, G.R.J., 1996. *The Late Devonian Mass Extinction - The Frasnian/Famennian*
754 *crisis.* Columbia University Press, New York.
- 755 McGhee, G.R., Jr., 2013. *When the invasion on land failed: the legacy of the Devonian*
756 *extinctions.* Columbia University Press, New-York.

- 757 Miller, K.G., Kominz, M.A., Browning, J.V., Wright, J.D., Mountain, G.S., Katz, M.E.,
758 Sugarman, P.J., Cramer, B.S., Christie-Blick, N., Pekar, S.F., 2005. The Phanerozoic
759 Record of Global Sea-Level Change. *Science* 310, 1293–1298.
- 760 Morrow, J., 2000. Shelf-to-basin lithofacies and conodont paleoecology across Frasnian-
761 Famennian (F-F, mid-Late Devonian) boundary, Central Great Basin (Western U.S.A.).
762 *Cou. Forsch.-Inst. Senckenberg* 219, 1-57.
- 763 Mottequin, B., Brice, D., Legrand-Blain, M., 2013. Biostratigraphic significance of
764 brachiopods near the Devonian–Carboniferous boundary. *Geol. Mag.* 151, 216-228.
- 765 Paul, D., Skrzypek, G., Forizs, I., 2007. Normalization of measured stable isotope
766 composition to isotope reference scale – a review. *Rapid Comm. Mass Spectr.* 21, 3006-
767 3014.
- 768 R Core Team, 2017. R: A language and environment for statistical computing. R
769 Foundation for Statistical Computing, Vienna, Austria. URL [https://www.R-](https://www.R-project.org/)
770 [project.org/](https://www.R-project.org/).
- 771 Sandberg, C.A., 1976. Conodont biofacies of late Devonian *Polygnathus styriacus* Zone in
772 western United States, in: Barnes, C.R. (Ed.), *Conodont Paleoecology*. Geol. Assoc.
773 Canada spec. Pap., Montreal, pp. 171-186.
- 774 Sandberg, C.A., Ziegler, W., Dreesen, R., Butler, J.L., 1988. Late Frasnian mass extinction:
775 conodont event stratigraphy, global changes, and possible causes. *Cour. Forsch.-Inst.*
776 *Senckenberg* 102, 263-307.
- 777 Sandberg, C.A., Morrow, J.R., Ziegler, W., 2002. Late Devonian sea-level changes,
778 catastrophic events, and mass extinctions. *Geol. Soc. America Spec. Pap.* 356, 473-487.
- 779 Schindler, E. 1993. Event-stratigraphic markers within the Kellwasser Crisis near the
780 Frasnian/Famennian boundary (Upper Devonian) in Germany. *Palaeogeogr.*
781 *Palaeoclimatol. Palaeoecol.* 104, 115-125.
- 782 Schlitzer, R., 2006. Ocean data view - 3.1.0. <http://odv.awi.de>
- 783 Schmidt, D., Caromel, A., Seki, O., Rae, J.W.B., Renaud, S., 2016. Morphological response of
784 planktic foraminifers to habitat modifications associated with the emergence of the
785 Isthmus of Panama. *Mar. Micropaleontol.* 128, 28-38.
- 786 Seddon, G., Sweet, W.C., 1971. An ecologic model for conodonts. *J. Paleont.* 45, 869-880.
- 787 Spalletta, C., Perri, M.C., Over, D.J., Corradini, C., 2017. Famennian (Upper Devonian)
788 conodont zonation: revised global standard. *Bull. Geosci.* 92, 1-27.

- 789 Stampfli, G.M., Hochard, C., V  rard, C., Wilhem, C., vonRaumer, J., 2013. The formation of
790 Pangea. *Tectonophysics* 593, 1-19.
- 791 Vennemann, T.W., Fricke, H.C., Blake, R.E., O'Neil, J.R., Colman, A., 2002. Oxygen isotope
792 analysis of phosphates: a comparison of techniques from analysis for Ag₃PO₄. *Chem.*
793 *Geol.* 185, 321-336.
- 794 Walliser, O.H., 1996. *Global events and event stratigraphy*. Springer Verlag, Berlin,
795 Heidelberg, New York.
- 796 Wilson, P.A., Norris, R.D., 2001. Warm tropical ocean surface and global anoxia during
797 the mid-Cretaceous period. *Nature* 412, 425-429.
- 798 Ziegler, W., 1962. Taxionomy und Phylogenie oberdevonischer Conodonten und ihre
799 stratigraphische Bedeutung. *Abhandlungen des hessischen Landesamtes f  r*
800 *Bodenforschung* 38, Wiesbaden, 166p.
- 801 Ziegler, W., Sandberg, C.A., 1984. *Palmatolepis*-based revision of upper part of standard
802 Late Devonian conodont zonation, in: Clark, D.L. (Ed.), *Conodont biofacies and*
803 *provincialism*. Geological Society of American special Paper, Boulder/Colorado, pp.
804 179-194.
- 805 Ziegler, W., Sandberg, C.A., 1990. The late Devonian standard conodont zonation. *Cour.*
806 *Forsch.-Inst. Senckenberg* 121, 1-115.

Figure captions

Figure 1. Paleogeographic reconstruction during the latest Famennian (simplified after Franke et al. 2017). BU: Buschteich; CT: Col des Tribes. Rectangles: investigated areas.

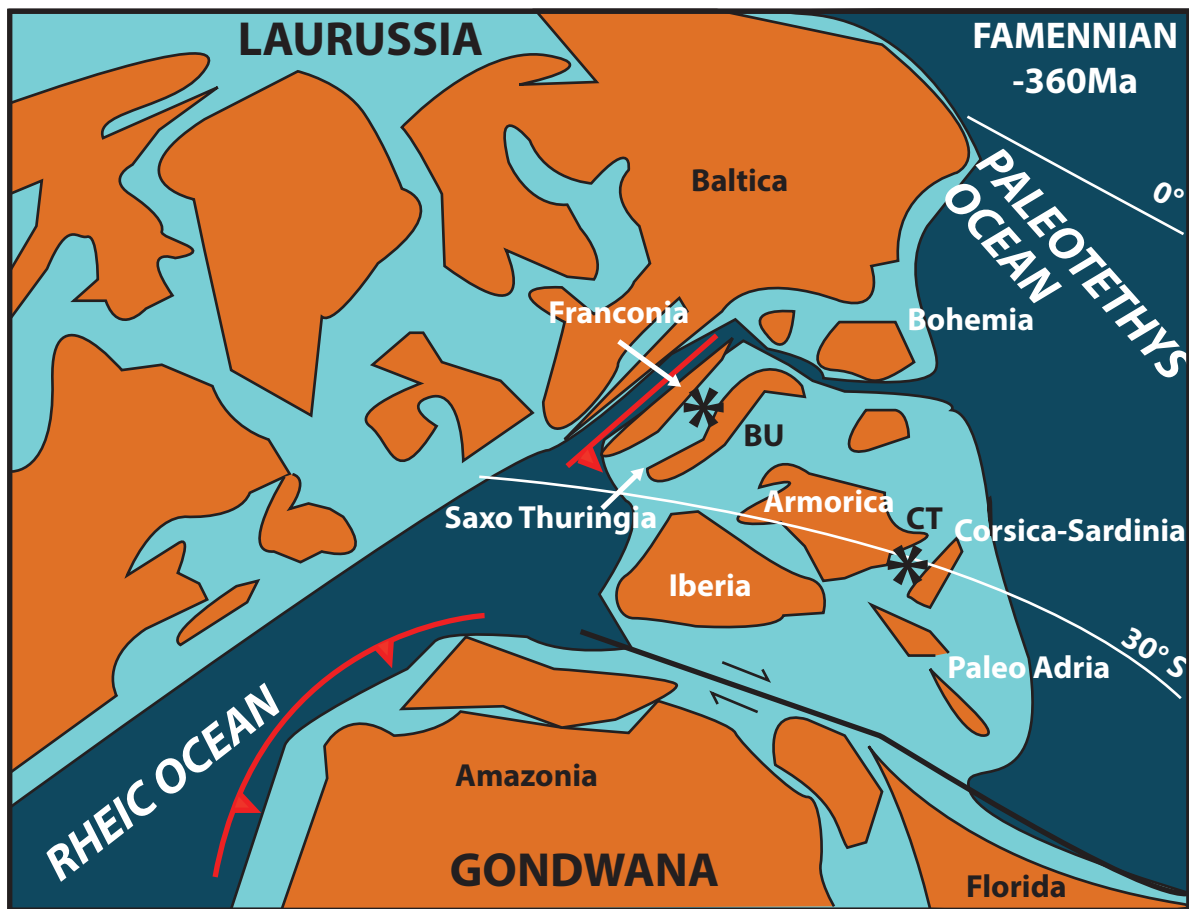
Figure 2. Age model allowing comparison of carbonate production rates between Buschteich (BU; red circles) and Col des Tribes (CT; green diamonds). Depth is given in meters. Conodont zonations according Ziegler and Sandberg (1990) on the right and Spalletta et al. (2017) on the left, absolute ages based on Becker et al. (2012). Each symbol corresponds to a sampled level. FRS: Frasnian. *Pa.*: *Palmatolepis*; *del.*: *delicatula*; *gl.*: *glabra*; *marg.*: *marginifera*; *gr.*: *gracilis*; *Sc.*: *Scaphignathus*; *v.*: *velifer*; *r.*: *rugosa*; *Ps.*: *Pseudopolygnathus*; *Bi.*: *Bispathodus*, *ac.*: *aculeatus*. In grey, zones which were not recognized in both sections.






Figure 3. Depositional model for the Col des Tribes (CT) and Buschteich (BU) sections during the Famennian.

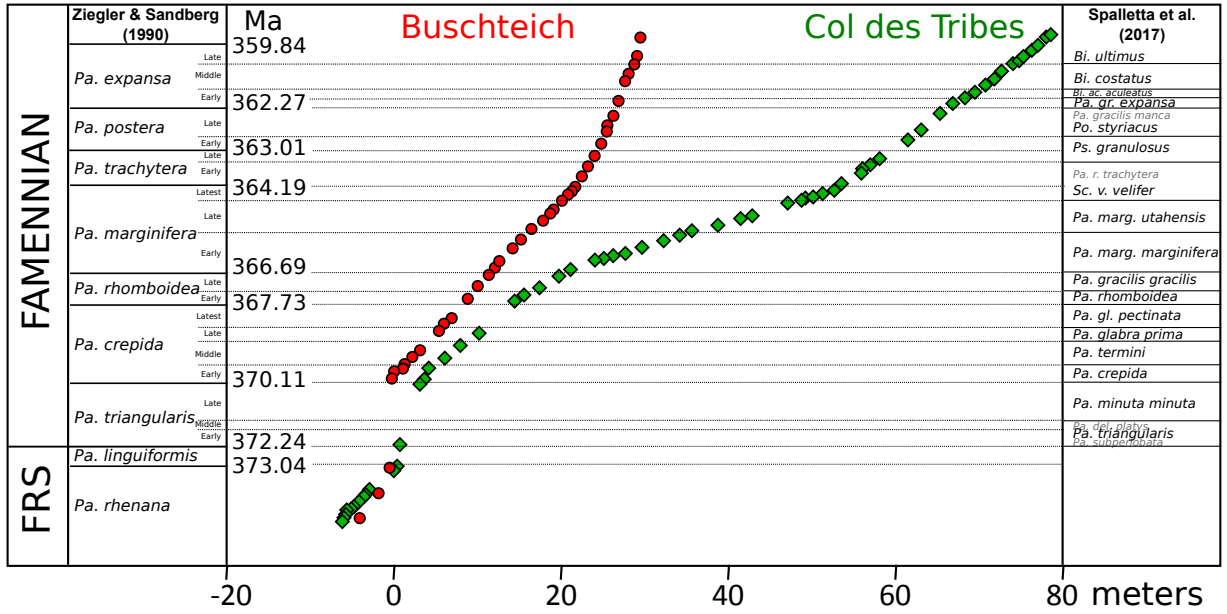
Figure 4. Famennian environmental changes and conodont assemblage variations in the Buschteich section (BU; Saxo-Thuringia) and Col des Tribes section (CT; Montagne Noire). A: Facies distribution for CT and BU from the deepest (1) to the shallowest (5). B: $\delta^{18}\text{O}$ in CT and BU samples, compared with data of Joachimski et al. (2009) from Thuringia (Kahlleite, blue circles) and the Montagne Noire (La Serre; grey diamonds). C. Variations of conodont assemblage through time depicted as variations along the first axis of the PCA on conodont genera percentages. Green diamonds: CT; red circles: BU. Abbreviations: see Figure 2.

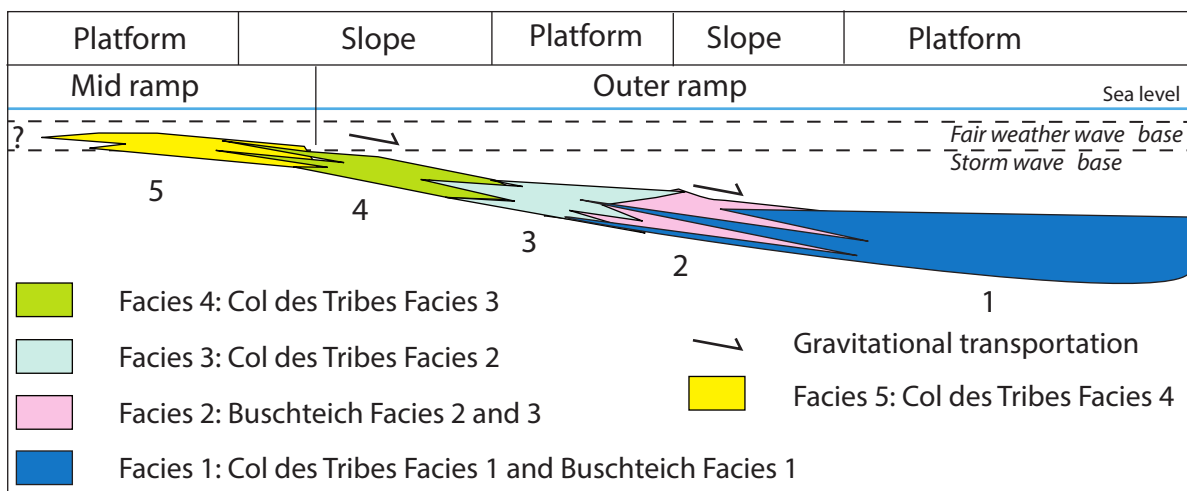
Figure 5. Conodont biofacies in CT and BU (after Girard et al. 2014; 2017). The proportions have been plotted against the age model. Note the absence of data (Gap) for the *Pa. linguiformis* to *Pa. crepida* zones at BU (white rectangle). *Scaphignathus* and *Alternognathus*: *Sc.*, *Siphonodella*: *Si.* on the figure.

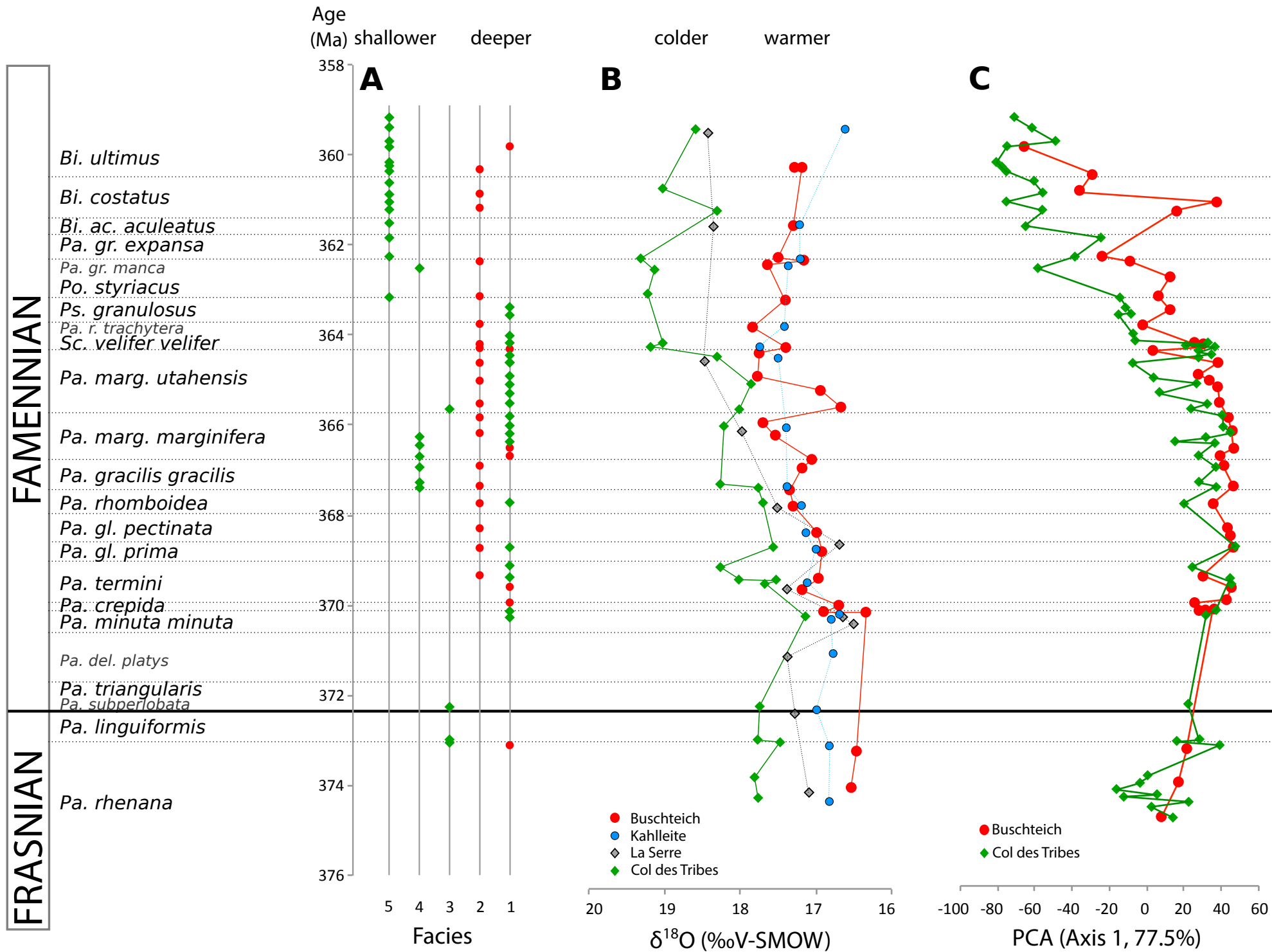
Figure 6. Principal component analysis of the variations in the percentages of the conodont genera in BU and CT. The first two axes of the PCA are represented (PC1 = 77.5%; PC2 = 18.3%). Upper left panel: contribution of the percentages of the different genera to the first two PC axes. Next panels: distribution of the different levels in the plane defined by the first two PC axes (PC1 = 77.5%; PC2 = 18.3%). The representation has been split by temporal zones (because of their limited sampling, *Pa. triangularis* to *Pa. gl. pectinata* Zones have been grouped). Each dot represents the assemblage in a level. CT: green diamonds, green diamonds with black outlines: levels from the *triangularis* and *minuta minuta* Zones; BU: red circles. *Pa.*: *Palmatolepis*; *gl.*: *glabra*; *gr.*: *gracilis*; *marg.*: *marginifera*; *Sc.*: *Scaphignathus*; *v.*: *velifer*; *r.*: *rugosa*; *Ps.*: *Pseudopolygnathus*; *Po.*: *Polygnathus*; *Bi.*: *Bispathodus*.

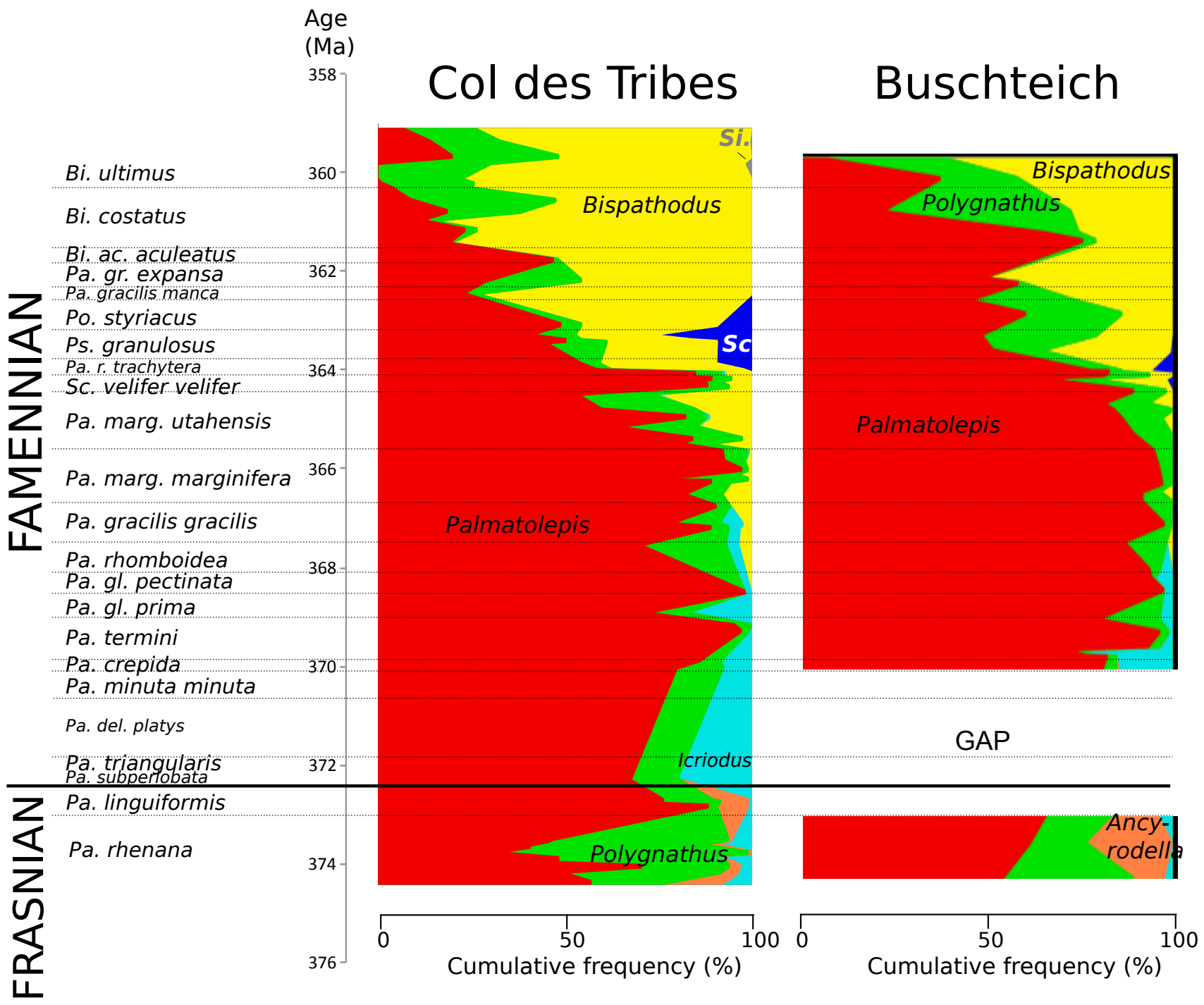


- | | | | | | |
|---|-------------------|---|-------------------|---|--------------|
|  | Continental areas |  | Marine shelf area |  | Oceanic area |
|  | Subduction |  | Fault | | |









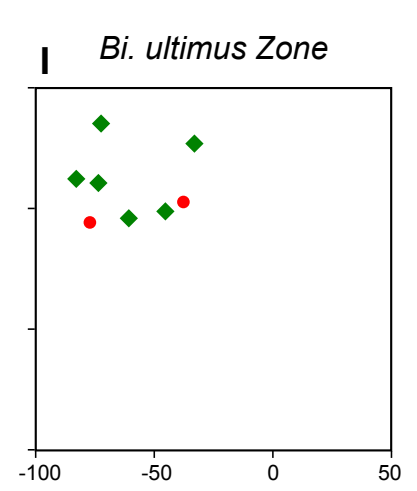
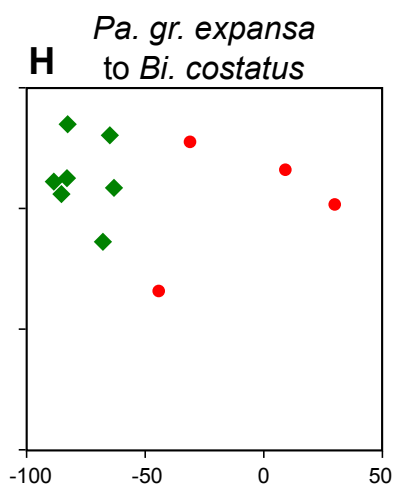
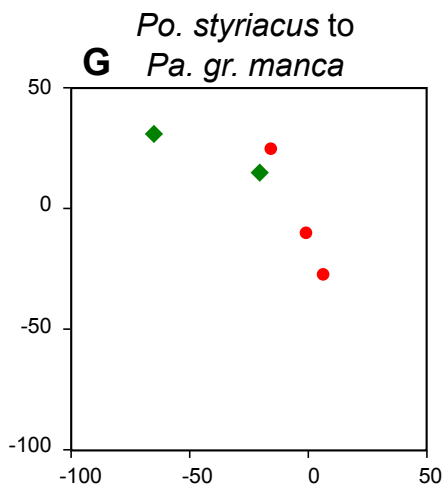
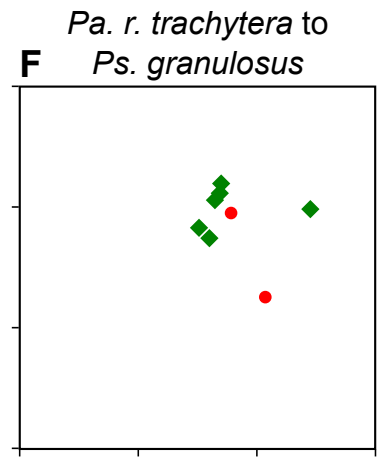
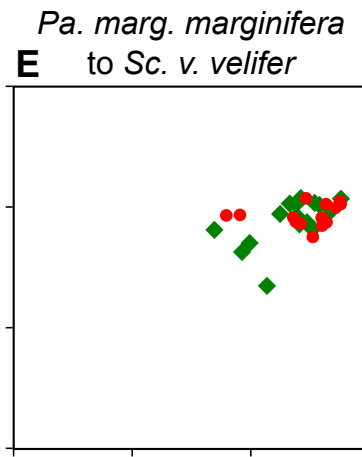
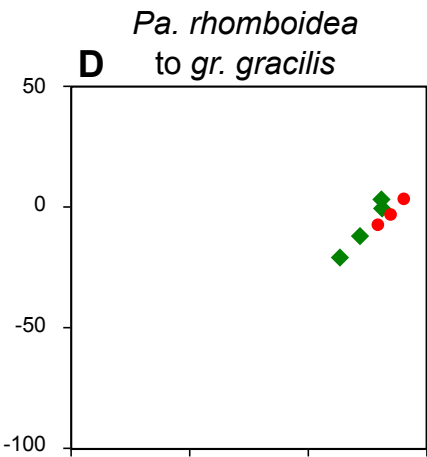
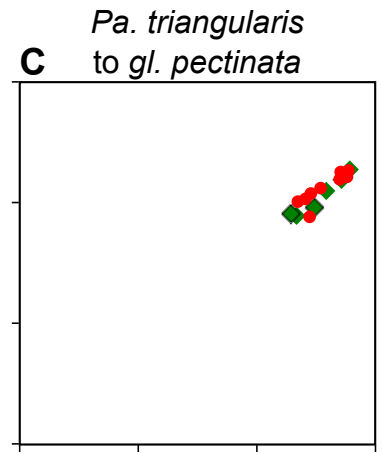
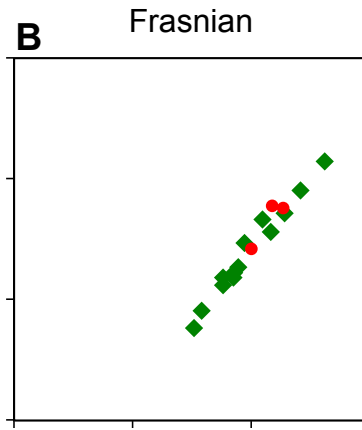
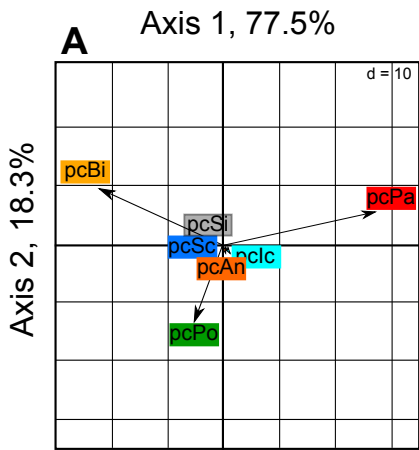


Table 1. Facies and environmental settings for the Col des Tribes and the Buschteich sections

FACIES	DIAGNOSTIC FEATURES	SEDIMENTARY FEATURES	STRATAL PATTERN	BIOCLASTS	DEPOSITIONAL SETTING	Girard et al. *2014 (CT) **2017 (BU)
Facies 1 : pelagic mudstone	Structureless lime mudstone with few bioclasts (2 – 10%)		Well stratified, dms thick	Pelagic ostracods and bivalves, goniatites, radiolarians, rare benthic ostracods, trilobites and crinoids	Outer ramp	Facies 1 at CT and BU
Facies 2: fine-grained turbidites	Laminated wackestone with pelagic fauna and scarce hardparts of benthic organisms	Mm to cm scale thick graded bedding, erosional surfaces at bottom	dm thick beds	Pelagic ostracods and bivalves, radiolarians, some transported benthic ostracods, blind trilobites brachiopods and crinoids	Distal turbidites in outer ramp interbedded within F1	Facies 2 and 3 at BU
Facies 3: pelagic wackestone	Structureless wackestone dominated by pelagic fauna and with 5 % benthic organisms	Pseudonodular structure	cm to dm thick beds	Pelagic bivalves and ostracods, diversified cephalopods, radiolarians, crinoids, benthic ostracods and trilobites	Outer ramp, shallower than F1 and F2	Facies 2 at CT
Facies 4: cephalopod wackestone to floatstone (griottes)	Reddish nodular to wavy laminated wackestone to floatstone with abundant goniatites	cm sized lime nodules coated by argillaceous and iron hydroxydes, intraformational breccias, rotated geopetal structures	Cm to dm thick beds	Goniatites, pelagic ostracods and bivalves, trilobites, brachiopods, crinoids and foraminifers	Slope in the upper outer ramp	Facies 3 at CT
Facies 5: wackestone with diversified fauna	Structureless to pseudonodular well stratified wackestone with pelagic and benthic organisms	Pseudonodular structure with cm to dm thick beds	cm to dm thick beds	Pelagic ostracods and abundant goniatites, trilobites, crinoids, brachiopods, gastropods, bivalves, foraminifers	Mid ramp	Facies 4 at CT

Table 2. Relationship between oxygen isotopes, microfacies, and conodont assemblages.

		CT+BU			CT			BU		
		n	R	p	n	R	p	n	R	p
$\delta^{18}\text{O}$	Facies	41	0.5023	0.0008	22	0.4107	0.0576	19	0.3149	0.1891
Conodont PC1	$\delta^{18}\text{O}$	51	-0.5304	6.2e-5	25	-0.5665	0.0031	26	-0.3039	0.1312
Conodont PC1	Facies	78	-0.6576	6.1e-11	52	-0.7058	5.1e-09	26	0.1799	0.3791
$\delta^{18}\text{O}$	Age	51	-0.5150	0.0001	25	-0.7532	1.388e-05	26	-0.7018	6.455e-05

Correlations between two variables using the Pearson's product-moment correlation, coefficient of correlation (R) and probability (p) are given. Analyses were performed for CT and BU combined, and CT and BU alone. Significant correlations marked in bold ($p < 0.05$).

Age is estimated based on the age model.

Table 3. Analyses of variance on oxygen isotopes and conodont proportions.

		CT+ BU			CT			BU			
	Dependent variable	Independent variable	n	Pve	p	n	Pve	p	n	Pve	p
(1)	$\delta^{18}\text{O}$	Age	51	30.5%	1.83E-09						
		Section		47.0%	4.06E-12						
		Age * Section		0.4%	0.375						
(2)	Conodont PC1	$\delta^{18}\text{O}$	41	6.1%	0.0311	22	9.0%	0.0316	19	11.2%	0.175
		Facies		22.3%	0.0001		33.6%	0.0003		0.5%	0.769

Two models were considered. (1) A model considered $\delta^{18}\text{O}$ as dependent variable, and age, section, and interaction (age * section) as effects. (2) A model considered PC1 based on conodont proportions in the assemblages as the dependent variable. The effects tested were $\delta^{18}\text{O}$ and facies score. Percentage of variance explained (pve) and probability (p) are given. Significant correlations marked in bold ($p < 0.05$).